Sensors & Actuators: B. Chemical 339 (2021) 129865

Contents lists available at ScienceDirect

Sensors and Actuators: B. Chemical

journal homepage: www.elsevier.com/locate/snb

A trigger-based aggregation of aptamer-functionalized gold nanoparticles for colorimetry: An example on detection of *Escherichia coli* O157:H7

Yuanyang Xie [a,b,1], Yu Huang [a,d,1,*], Jiye Li [a,d], Jiangling Wu [c,*]

[a] Chongqing Institute of Green and Intelligent Technology, Chinese Academy of Sciences, Chongqing, 400714, China
[b] Department of Physics and London Centre for Nanotechnology, King's College London, Strand, London, WC2R 2LS, UK
[c] Department of Clinical Laboratory, University-Town Hospital of Chongqing Medical University, Chongqing, 401331, China
[d] University of Chinese Academy of Science, Beijing, 100049, China

ARTICLE INFO

Keywords:
Escherichia coli O157:H7
Gold nanoparticle
Colorimetric sensor
Localized surface plasmon resonance
pH regulation

ABSTRACT

A pH-triggered colorimetric assay has been established by using aptamer anchored gold nanoparticles to detect *Escherichia coli* O157:H7 (*E. coli* O157:H7). Gold nanoparticles (AuNPs) functionalized by aptamer via thiol groups were used as probes (HS-Apt@AuNPs).Solvents of HCl (acid), NaOH (alkaline) and $MgCl_2$ (nearly neutral) were used as triggers to initiate the movement of HS-Apt@AuNPs in the presence of *E. coli* O157:H7 bacteria respectively. Due to the pH effect of trigger on the surface charges of *E. coli* O157:H7 and the contribution of aptamer to capture *E. coli* O157:H7, the movement of HS-Apt@AuNPs with the presence of *E. coli* O157:H7 exhibit dispersion and aggregation respectively, which leads the change of colorimetric signal to an opposite direction. Taking the solvent of NaCl frequently used as trigger for gold nanoparticle based colorimetric sensor into consideration, the utilization of pH dependent triggers provide an alternative for this kind of trigger-based sensor. Design of gold nanoparticle-based colorimetric biosensing assay suiting a wide range of trigger is more flexible for specific diagnosis. These results demonstrate a great potential to design bacterial sensor with high sensitivity to defend public health.

1. Introduction

Escherichia coli O157:H7 (*E. coli* O157:H7), a kind of highly infective pathogenic bacteria, is a leading threat to public health [1]. It is a widespread food-borne pathogen and the infective dose is as low as 50–100 cells. Each year, more than 73,000 people are caused from slight to life-threatening diarrhea due to these bacteria in the United States. The infective source is ranging from contaminated food to water [2]. Although a number of methods, including SERS [3], immune chromatographic test strips [2], electrochemical detection [4] and lateral flow immunoassay [5] have been developed to detect *E. coli* O157:H7, the requirement of time-consuming steps, expensive instruments and reagents of these methods limit their widely application. An accurate, rapid and simple analytical method is still required for public health control and prevention authority to screening of large quantity of samples on field.

Aptamers are single-stranded RNA or DNA oligonucleotides, which could specifically bind to targets with high specificity and affinity [6]. They are obtained by the SELEX method in vitro and have a high affinity for a wide range of target, from small molecules, metal ions, organic dyes, mycotoxin and to proteins, or even whole cells such as bacteria [7]. Due to the advantage of aptamer compared to antibodies, aptamers have gained a great deal of attention for the development of aptamer-based colorimetric sensor. Aptamer plays a significant role as a recognition element and a transducer to receive signal originated from biological and chemical specimen. Gold nanoparticles (AuNPs), especially aptamer-modified AuNPs, have been widely used owing to their catalytic activity and localized surface plasmon resonance (LSPR) [8,9]. Owning to their unique optical properties, colloidal gold nanoparticles are commonly utilized to develop colorimetric assay. The colorimetric assays established by aptamer-modified AuNPs are mainly based on aggregation of AuNPs, which results in a red-to-blue color change [10]. Control of dispersion and aggregation behavior of colloidal gold nanoparticles is a key factor to implement gold nanoparticles based colorimetric sensing platform [11].

In general, the colorimetric sensor is categorized by the

* Corresponding author.
E-mail addresses: huangyu@cigit.ac.cn (Y. Huang), wjl135@126.com (J. Wu).
[1] These authors contributed equally to this work.

https://doi.org/10.1016/j.snb.2021.129865
Received 3 January 2021; Received in revised form 2 March 2021; Accepted 26 March 2021
Available online 29 March 2021

immobilization methods of aptamer on gold nanoparticle surface, which are dependent on whether the anchor group is utilized or not. In the presence of target, the aptamer immobilized on the surface of gold nanoparticles without the function of anchor group was separated from gold nanoparticle and bound to its target. This is ascribed to a competitively attractive force of gold nanoparticle and targets toward aptamer [12]. On the other hand, the aptamer immobilized on gold nanoparticle with anchor groups, such as thiol and polyadenine (polyA), can be constantly tethered on AuNPs due to strong bonds [13]. The AuNPs with anchored aptamer, denoted as a-ssDNA&AuNPs, have a higher degree of stabilization and its dispersion/aggregation behavior is more flexible to be controlled than the AuNPs immobilized with aptamer due to the electrostatic interaction, denoted as n-ssDNA&AuNPs [14]. Furthermore, the a-ssDNA&AuNPs can be used as programmable atom-like nanoparticles to design diversified structures made up of several single nanoparticle, which is the result of base complementary of ssDNA anchored on the surface of gold nanoparticle [13]. It has shown a great application potential in a number of chemicals, biological and environmental sensing fields.

Crosslinking aggregation and non-crosslinking aggregation are two sensing mechanism of colorimetric sensor based on aptamer-modified AuNPs. The crosslinking aggregation is defined as the attraction of several single gold nanoparticles due to the base complementary of ssDNAs. The reason for non-crosslinking aggregation is that the introduction of targets undermines the stability of aptamer-modified AuNPs [15]. The aggregation of AuNPs is triggered by the presence of salt and its aggregative degree could be controlled by salt concentration [16]. Different from crosslinking aggregation, the approach of non-crosslinking aggregation does not require complicated usage of nanoprobes and strict temperature control [17]. Hence, the mechanism of non-crosslinking aggregation has been widely used to design colorimetric sensors. The non-crosslinking aggregation method of aptamer-modified AuNPs is a simple and effective way to build novel assays. Since Li et al. [18] firstly established the AuNPs-based colorimetry by non-crosslinking aggregation, n-ssDNA&AuNPs typed sensor had been investigated in numerous cases for the development of detecting assays [19]. However, a-ssDNA&AuNPs typed sensor has less development compared to its counterpart. One of the main reasons is the lack of a mature theory system as a guideline to establish novel and efficient sensing strategies. The application of AuNPs colorimetric applications is significantly dependent on the stability degree of colloid system. The electrostatic stabilization has been determined as the single factor to maintain the stability of n-ssDNA&AuNPs typed colorimetric sensor [18]. The release of ssDNA absorbed on surface of AuNPs weakens the surface charge of AuNPs and disturbs the stability of colloid system. However, the factors used to maintain the stability of a-ssDNA&AuNPs typed colorimetric sensor has yet understood. Either electrostatic or steric stability may contribute to the aggregation/dispersion mechanism [20,21].

In this paper, thiol-modified *E. coli* O157:H7 aptamer was immobilized on the surface of gold nanoparticle, called HS-Apt@AuNPs, for analysis of *E. coli* O157:H7. This aptamer-based colorimetric assay is categorized as aforementioned a-ssDNA&AuNPs typed sensor. Both pH and ionic strength are crucial parameters to control the stabilization of colloid system. The change in pH of solvent has an influence to modify the surface charge of *E. coli* O157:H7, and then consequently the signal change of colorimetric sensor. The solvent of HCl (acid), NaOH (alkaline) and $MgCl_2$ (nearly neutral) were chosen as triggers to initiate the signal change of colorimetric sensor by disturbing the stability of colloidal system. The incubation of *E. coli* O157:H7 and HS-Apt@AuNPs by using PBS buffer was implemented before the addition of three triggers respectively. Compared to the resonance wavelength of HS-Apt@AuNPs colloid only initiated by the presence of HCl, the addition of both HCl and *E. coli* O157:H7results in a greater aggregation of HS-Apt@AuNPs, and leads the resonance wavelength a further red-shift. In contrast, the addition of NaOH or $MgCl_2$, with *E. coli* O157:H7 induce dispersion of HS-Apt@AuNPs. This leads to a spectral blue-shift compared to its initial stage, where only NaOH or $MgCl_2$ is present in HS-Apt@AuNPs colloid. No matter what trigger was used, the degree of change in color becomes more and more significant with an increase in the concentration of *E. coli* O157:H7 until the concentration of *E. coli* O157:H7 surpasses a certain level. The extinction ratio of this aptamer-anchored gold nanoparticle sensor exhibited a linear correlation with *E. coli* O157:H7 concentration. The detection limits of 40.46, 94.08 and 147.6 CFU/mL were obtained by using HCl (acid), NaOH (alkaline) or $MgCl_2$ (nearly neutral) respectively. Moreover, the mechanism for triggers with a wide range of pH to initiate the detection has been explored in detail. The utilization of aggregation/dispersion change of aptamer-anchored gold nanoparticle sensor by using trigger with different pH according to practical situation could significantly improve the detection accuracy and efficiency.

2. Materials and methods

2.1. Materials

Phosphate buffered saline tablet and hydrogen tetrachloroaurate (III) trihydrate ($HAuCl_4{\cdot}3H_2O$) were obtained from Sigma. Trisodium citrateanhydrous was procured from Alfa Aesar. Sodium acetate trihydrate was purchased from BBI Life Sciences. Tris(2-carboxyethyl) phosphine hydrochloride (TCEP), acetate and $MgCl_2$ were purchased from Aladdin. HCl, NaOH and NaCl were purchased from Chongqing Chuandong Chemical (Group) Co., Ltd. The oligonucleotides were synthesized and HPLC-purified by Sangon Biotech Co., Ltd (Shanghai, China). The base sequences are listed in Table S1. All reagents were of at least analytical grade. The water used throughout the work had resistivity higher than 18 $M\Omega\,cm^{-1}$.

2.2. Culture of E. coli O157:H7

E. coli O157:H7, staphylococcus aureus, pseudomonas aeruginosa and *E. coli* ATCC35218 were obtained from University–Town Hospital of Chongqing Medical University. Stock cultures in 25 % glycerol were maintained frozen at −80 ℃. All bacteria was inoculated into nutrient broth (NB) and grown for 18−24 h at 37 ℃ with constant agitation. The cultures containing bacteria were centrifuged at 4000 rpm for 5 min and then washed and resuspended with phosphate-buffered solution (PBS) (10 mM, pH 7.4). The prepared bacteria were inactivated by boiling at 90 ℃ for 10 min and stored at 4 ℃ for further use. For bacterial enumeration, a scattered light turbid meter was used to determine the bacterial densities. The actual amount of bacteria was then determined according to the optical density measured at the wavelength of 600 nm. Finally, the suspension was immediately diluted to 1.0×10^2 to 10.0×10^3 CFU/mL for measurement.

2.3. Apparatus

The UV–vis extinction spectra were monitored by a custom-made extinction spectroscopy shown in Fig. S1. In the spectroscopy system, a tungsten halogen lamp (HL-2000-HP, Ocean Optics) and a spectrometer (HR4000, Ocean Optics) were employed as light source and detector respectively. Then, the quartz cuvette with a path-length of 1 cm in dark was used as sample cell and the extinction from the samples was analyzed by programs written in C++ and Matlab. Scanning electron microscope (SEM) images were obtained by field emission scanning electron microscopy (JEOL JSM-7800 F). The zeta potential was obtained by Malvern Zetasizer Nano ZS.

2.4. Modification of the aptamer

The aptamer of *E. coli* O157:H7 with length of 72 nucleotides has shown high affinity and specificity [22]. All mismatched nucleotides

were modified from the original 72-mer *E. coli* O157:H7 specific aptamer. The predicated secondary structures of all nucleotides were obtained from the Mfold web server (http://www.unafold.org/DNA_form.php).

2.5. Preparation of aptamer-anchored gold nanoparticle sensor

AuNPs with ~12 nm in diameter were synthesized via previously described sodium citrate reduction methods [23]. Briefly, 1.5 mL of 1 % trisodium citrate solution was added to 10 mL 1 mM $HAuCl_4$ boiling and vigorously stirred. The mixed solution was kept stirring and heating for 20 min, cooled down to room temperature, filtered by a 0.22 mm PES Syringe Filters and stored at 4 ℃ before functionalization. Thiol-*E. coli* O157:H7 specific functionalized gold nanoparticles (HS-Apt@AuNPs) were prepared with a method reported in literature [23]. Firstly, 3 μL of 1 mM 5'-thiol aptamer were activated by mixing with 0.5 μL of 10 mM freshly prepared TCEP and 0.5 μL of 500 mM acetate buffer (pH5.2) at room temperature for 1 h. Then this solvent was added to 3 mL prepared gold nanoparticles solution. The mixture was incubated in a drawer at room temperature for at least 16 h. Next, in order to maximize the amount of aptamer loading on the surface of gold nanoparticles, 30 μL of 500 mM Tris acetate buffer (pH8.2) and 300 μL of 1 M NaCl were added dropwise and stored in a drawer at room temperature for at least 24 h. The concentration of HS-Apt@AuNPs was estimated by Lambert-Beer law, A=εcl (the molar extinction coefficient of AuNPs at 520 nm was 2.7×10^8 M^{-1} cm^{-1}) [24].The procedure to immobilize mismatched nucleotides on the surface of AuNPs is the same as that of *E. coli* O157:H7 specific aptamer.

2.6. Detection of E. coli O157:H7

The detection procedure of *E. coli* O157:H7 was carried out as follows: 1.5 mL PBS buffer with different concentrations of *E. coli* O157:H7 and 45 μL HS-Apt@AuNPs were added to a 2 mL micro centrifuge tube, shaken thoroughly and incubated 30 min at room temperature. Then, $MgCl_2$ (0.717 M), HCl (1 M) or NaOH(12 M) was added to initiate detection respectively. The volume of $MgCl_2$, HCl or NaOH was adjusted to optimize the sensitivity. After 30 min of trigger addition, the extinction spectrum was recorded from 400 nm to 800 nm. The ratio of extinction reading at 620 nm to that at 520 nm (E_{620nm}/E_{520nm}) was used for quantitative analysis. All data was collected from at least three independent measurements. The specificity test was performed as above-mentioned procedure with *E. coli* O157:H7 changed by other bacteria.

2.7. Detection of spiked water samples

The tap water was spiked with *E. coli* O157:H7 of 2.0×10^2, 8.0×10^2 and 3.0×10^3 CFU/mL respectively. The 4 mL spiked samples were centrifuged for 10 min at 10 000 *g*. The supernatants were discarded and then PBS (pH 7.4) was added to be 4 mL. The centrifugation repeated at least 3 times. 4 mL pretreated samples were added with 120 μL HS-Apt@AuNPs to incubate. After 30 min, 1.5 mL mixed samples were detected with the addition of $MgCl_2$ and HCl as trigger separately.

In order to evaluate the interferences of mixed bacteria presenting in spiked water on this proposed method, 4 mL tape water with the mixture of *E. coli* O157:H7, staphylococcus aureus, *E. coli* ATCC35218, pseudomonas aeruginosa were prepared at first. The concentration of each bacterium was prepared as 5.0×10^2 and 1.0×10^3 CFU/mL respectively. Then the testing procedure was carried out as the same as above-mentioned one.

3. Results and discussion

3.1. Characterization of HS-Apt@AuNPs

Fig. 1 depicts the normalized extinction spectra of AuNPs and HS-Apt@AuNPs respectively. The extinction peak of AuNPs is at 520 nm. The immobilization of HS-Aptamer on AuNPs makes their extinction peak nearly 8 nm red-shift to 528 nm. The red-shift of extinction indicates that the aptamer of *E. coli* O157:H7 had successfully anchored on the surface of AuNPs, which results in the dielectric constant change of surrounding medium of gold nanoparticle [25].

To further confirm the function of *E. coli* O157:H7 aptamers-anchored AuNPs, gel electrophoresis route was utilized to explore the interaction between HS-Apt@AuNPs and *E. coli* O157:H7. In the presence of low-concentration *E. coli* O157:H7 (1.8×10^4 CFU/mL), an obvious decrease in shift of red-color band location of HS-Apt@AuNPs in gel was observed in Fig. 2. Moreover, the running shift of HS-Apt@AuNPs was further reduced when the concentration of *E. coli* O157:H7 was increased to be 3.6×10^4 CFU/mL. The running shift of HS-Apt@AuNPs decreased with an increase of *E. coli* O157:H7 concentration could be ascribed to the enhanced loading amount of *E. coli* O157:H7 increasing the weight and size of HS-Apt@AuNPs clusters presenting at the surface of *E. coli* O157:H7 [26]. More time is required to separate HS-Apt@AuNPs clusters from these bacteria and move with electrical force. Then higher concentration of *E. coli* O157:H7 would result in slower move of larger HS-Apt@AuNPs clusters. The morphological structure of aptamers-anchored AuNPs/*E. coli* O157:H7 complex was characterized by using SEM as shown in Fig. S2. Aptamers-anchored AuNPs conjugated with *E. coli* O157:H7 and they scattered randomly on the surface of *E. coli* O157:H7 bacteria.

3.2. Colorimetric test for E. coli O157:H7 with $MgCl_2$ trigger

The strategy of a-ssDNA&AuNPs typed colorimetric sensor is that salt is used as a trigger to modify the aptamer-induced protection when aptamer hybridized with its target [18,27].Generally speaking, aptamers anchored on the surface of AuNPs provide electrostatic repulsion between individual gold nanoparticle to resist certain amount of salt-induced aggregation. Salts with multivalent ions would provide enhanced ionic strength compared to monovalent ion salt at the same concentration condition. Therefore, $MgCl_2$ with bivalent cation is a better choice used as trigger compared to conventional NaCl, because less amount of salt is required, and the volume change of mixture induced by the addition of $MgCl_2$ is negligible.

Simple preparation, rapid and sensitive response of a sensor is an

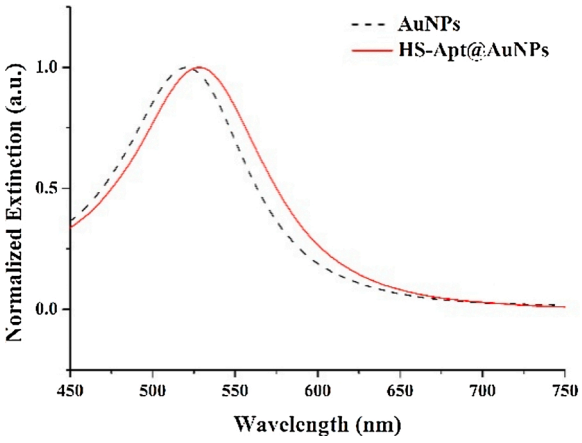

Fig. 1. Normalized extinction spectra of AuNPs (black dash line) and HS-Apt@AuNPs (red solid line) (For interpretation of the references to colour in this figure legend, the reader is referred to the web version of this article.).

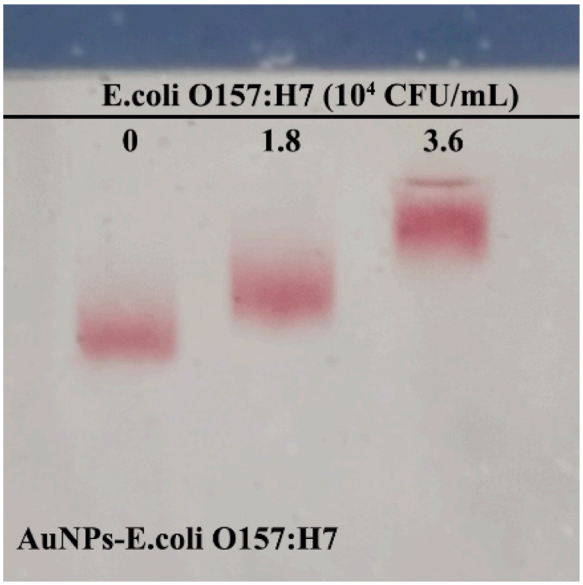

Fig. 2. Gel electrophoresis results of aptamer functionalized AuNPs with various concentration of *E. coli* O157:H7(from 0, 1.8×10^4 to 3.6×10^4 CFU/mL) after 30 min incubation. The condition for gel electrophoresis: 3 % agarose, 5 V/cm, 0.5 × PBS, 30min.

advantage for low cost and real-time detection of *E. coli* O157:H7.45 μL HS-Apt@AuNPs solution was added to1.5 mL PBS buffer with *E. coli* O157:H7 of 3.6×10^3 CFU/mL and without *E. coli* O157:H7 respectively. After incubating for 5 min, 45 μL of $MgCl_2$ (0.717 M) was introduced to the mixtures, followed by extinction characterization. The aggregation/dispersion kinetics of this proposed sensor were examined by measuring the extinction ratio of E_{620nm}/E_{520nm} at room temperature as shown in Fig. 3A.It can be seen that in the first 10 min, the extinction ratio increased rapidly along with the time passed by. Then, the growth of extinction ratio slowed down and approached plateau since about 30 min. The magnitude of extinction ratio of HS-Apt@AuNPs induced by the presence of *E. coli* O157:H7 is much smaller than its counterpart. This could be revealed that the attachment of HS-Apt@AuNPs on the bacterial cell surface was promptly finished in the initial stage. The presence of *E. coli* O157:H7 could stabilize HS-Apt@AuNPs solution against aggregation or even disperse them.

In addition, incubation time was also investigated to improve the measurement reproducibility. A series of incubation time ranging from 0 to 50 min were selected and the extinction ratio of HS-Apt@AuNPs monitored at the 30th minute after the addition of 45 μL of $MgCl_2$ (0.717 M) are shown in Fig. 3B. The extinction ratio gradually decreases with an increase of incubation time and it tends to be stable after about 30 min reaction. To compromise between repeatability, reproducibility and a highly efficient and sensitive assay, therefore, optimum time of 30 min for incubation and 30 min for reaction was chosen in the subsequent work.

The effect of $MgCl_2$ volumes on the response of HS-Apt@AuNPs solution was implemented at the volume range of 40,45,47,50,52,55 μL of 0.717 M $MgCl_2$. Based on the spectra of HS-Apt@AuNPs solution with and without the addition of *E. coli* O157:H7 at each volume, the plot of E_{620nm}/E_{520nm} was sorted out(Fig. 4). From the plot, the measurable extinction ratio monotonously increases with an increase of $MgCl_2$ volumes, while the difference between the extinction ratios associated with and without *E. coli* O157:H7 approach the greatest value at 50 μL and then decrease slightly from 52 to 55 μL. This indicated that 50 μL of $MgCl_2$ (0.717 M) is able to enhance the dispersion degree of HS-Apt@AuNPs in the presence of *E. coli* O157:H7 and assemble HS-Apt@AuNPs in the absence of *E. coli* O157:H7 more greatly compared to that of other volume of $MgCl_2$. The different extinction ratio induced by the addition of *E. coli* O157:H7 is maximum when 50 μL of $MgCl_2$ (0.717 M) is used as trigger. Therefore, 50 μL of $MgCl_2$ (0.717 M) is chosen in the following work since it could result in the maximum difference of extinction ratio (E_{620nm}/E_{520nm}) induced by the presence of *E. coli* O157:H7.

In order to quantitatively detect *E. coli* O157:H7 using this HS-Apt@AuNPs colorimetric sensor, a series of reactions containing various amounts of target bacteria were employed. As shown in Fig. 5A, along with the increase of the *E. coli* O157:H7 concentration, the extinction spectra show a blue-shift. The extinction at 520 nm gradually increased, while the broad extinction (600−750 nm) gradually

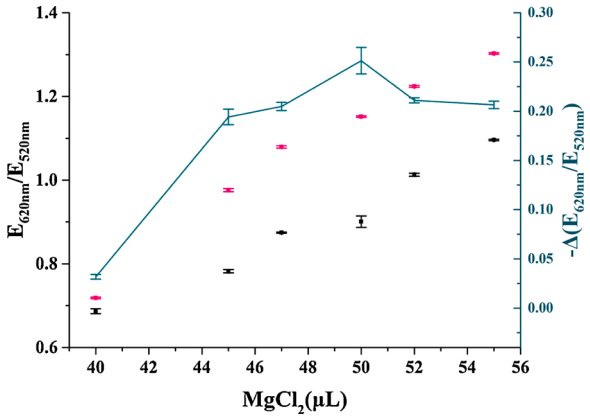

Fig. 4. The effect of volumes of $MgCl_2$ (0.717 M) used as trigger on detecting *E. coli* O157:H7 of 3.6×10^3 CFU/mL. Black and pink color represent sample with and without *E. coli* O157:H7 bacteria respectively.

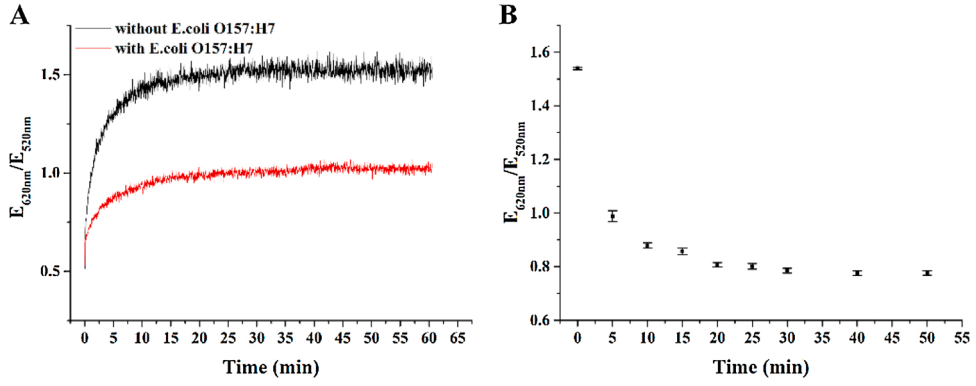

Fig. 3. (A) Response of HS-Apt@AuNPs monitored after the addition of $MgCl_2$ with and without *E. coli* O157:H7incubated for 5 min. (B) Extinction ratio of E_{620nm}/E_{520nm} with various incubation times of HS-Apt@AuNPs with *E. coli* O157:H7 of 3.6×10^3CFU/mL.

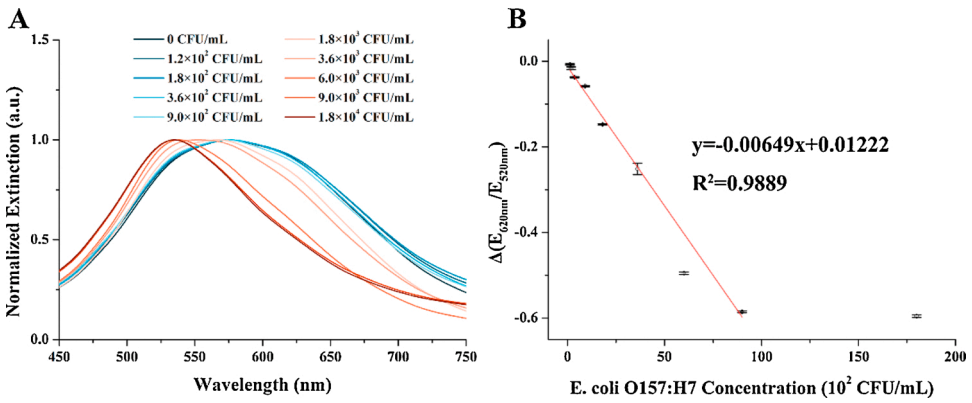

Fig. 5. Performance of HS-Apt@AuNPs based colorimetric sensor for the detection of *E. coli* O157:H7 with 50 μL 0.717 M $MgCl_2$ used as trigger. (A) Extinction spectra of HS-Apt@AuNPs with various concentrations of *E. coli* O157:H7. (B) Corresponding differential extinction ratio, $\Delta(E_{620nm}/E_{520nm})$, as a function of *E. coli* O157:H7concentrations. The straight line is a linear regression between 1.2×10^2 to 9.0×10^3 CFU/mL of *E. coli* O157:H7.

decreased. In order to characterize the influence of *E. coli* O157:H7 bacteria on the spectra, a differential extinction ratio, $\Delta(E_{620nm}/E_{520nm})$, is defined as

$$\Delta(E_{620nm}/E_{520nm}) = (E_{620nm}/E_{520nm})p - (E_{620nm}/E_{520nm})a \quad (1)$$

where $(E_{620nm}/E_{520nm})p$ and $(E_{620nm}/E_{520nm})a$ represent the extinction ratio of E_{620nm}/E_{520nm} monitored in the presence and absence of *E. coli* O157:H7 bacteria respectively.

The differential extinction ratio shown in Fig. 5B decreases linearly with an increasing concentration of *E. coli* O157:H7 was observed in the concentration range from 1.2×10^2 to 9.0×10^3 CFU/mL and a detection limit of 94.08 CFU/mL, with a slope of -0.00649 and a linear response of $R^2 = 0.9889$. These results clearly show that the optical extinction of HS-Apt@AuNPs colorimetric sensor is sensitive to *E. coli* O157:H7.

3.3. Colorimetric test for E. coli O157:H7 with NaOH/HCl as trigger

Since this detection principle was based on either electrostatic or steric stability with regard to a-ssDNA&AuNPs typed colorimetric sensor, the value of pH would be a crucial factor in the formation of hydrogen bonds and the determination of surface charge polarity. AuNPs colloid is generally stable in an environment with high value of pH [28]. However, extremely high ionic strength would reduce the electrical double layer around HS-Apt@AuNPs and destabilize HS-Apt@AuNPs colloid. Thus, solvent of NaOH with concentration as high as 12 M and HCl with concentration of 1 M was then selected as triggers to investigate the pH effect on the response of HS-Apt@AuNPs solution to *E. coli* O157:H7 respectively, since they are able to disturb the stability of HS-Apt@AuNPs colloid. The volume optimizing procedure of these triggers to maximize optical response of HS-Apt@AuNPs colorimetric sensor to *E. coli* O157:H7 is as similar as above-mentioned that of $MgCl_2$.

The addition of NaOH immediately increased the pH of HS-Apt@AuNPs colloid. Increasing volume of NaOH from 15 to 50 μL led the pH of reacted solvent jump to the range of 13.01−13.48. This pH value was higher than the isoelectric point of *E. coli* O157:H7 [29]. At this value, negative charged HS-Apt@AuNPs could be dispersed from negative charged *E. coli* O157:H7. As shown in Fig. 6A, the differential extinction ratio of this sensor $\Delta(E_{620nm}/E_{520nm})$ increases firstly and then decreases with an increasing NaOH volume when the concentration of *E. coli* O157:H7 was constantly set at 3.6×10^3 CFU/mL. Larger volume of NaOH resulted in a significant decrease in response. Therefore, 20 μL NaOH was selected as the volume of trigger. The working response and performance characteristics of HS-Apt@AuNPs colorimetric sensor were evaluated by colorimetry. Fig. 6B shows a linear response of sensor when different concentrations of bacteria, from 1.2×10^2 CFU/mL to 9.0×10^3 CFU/mL, were set to react. This yielded a sensitivity of 0.507 CFU/mL and a detection limit of 147.6 CFU/mL for measurement of *E. coli* O157:H7.

On the contrary, the addition of both HCl and *E. coli* O157:H7 would aggregate HS-Apt@AuNPs colloid and lead a spectral red-shift. Red-shift spectra led to an increase in extinction reading at 620 nm region along with the concomitant decrease in the intensity of extinction reading at 520 nm. Then, the sign of $\Delta(E_{620nm}/E_{520nm})$ turned to be positive compared to that of $MgCl_2$ and NaOH used as trigger. The effect of HCl

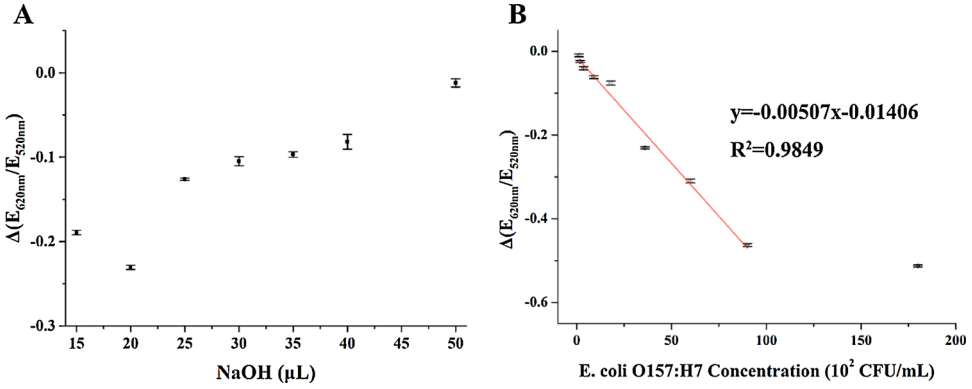

Fig. 6. (A) The effect of volumes of NaOH(12 M) used as trigger on detecting *E. coli* O157:H7of 3.6×10^3 CFU/mL (B) Differential extinction ratio, $\Delta(E_{620nm}/E_{520nm})$, as a function of *E. coli* O157:H7concentrations when 20 μL NaOH was selected as trigger. The straight line is a linear regression between 1.2×10^2 CFU/mL to 9.0×10^3 CFU/mL of *E. coli* O157:H7.

volume on the performance of sensor was carried out at the condition of *E. coli* O157:H7 3.6×10^3 CFU/mL. The pH of reacted solvent was decreased from 2.23 to 1.67 by increasing the HCl volume from 18 to 27 μL. The plot of $\Delta(E_{620nm}/E_{520nm})$ as a function of HCl volume shown in Fig. 7A indicated that 25 μL HCl (1 M) is an optimum parameter. To quantitatively analyse *E. coli* O157:H7, a typical plot of differential extinction ratio $\Delta(E_{620nm}/E_{520nm})$ versus *E. coli* O157:H7 concentration ranging from 1.2×10^2 to 18×10^3 CFU/mL is shown in Fig. 7B. It is found that the extinction spectrum of HS-Apt@AuNPs exhibited a red shift with an increase in concentration of *E. coli* O157:H7 up to 6.0×10^3 CFU/mL and then shifted to short wavelength region at higher concentration of *E. coli* O157:H7. A linear response in the colorimetric detection for the concentration of *E. coli* O157:H7 was found between 1.2×10^2 and 3.6×10^3 CFU/mL, with a slope of 0.942 and a correlation coefficient of $R^2 = 0.9765$. This HS-Apt@AuNPs colorimetric sensor triggered by HCl could detect the target *E. coli* O157:H7 with a detection limit of 40.46 CFU/mL.

3.4. Comparison of colorimetric test for E. coli O157:H7

The performance of this proposed method and other sensors for the detection of *E. coli* O157:H7 are summarized in Table S2. The working range and theoretical LOD, calculated as three times the signal-to-noise ratio are comparable, and even better than some counterparts. This proposed method had proved that acidic, alkaline and neutral triggers are able to be utilized to implement colormetric *E. coli* O157:H7detection with the support of gold nanoparticle. It provides a flexible and cost-effective way to detect *E. coli* O157:H7 by either shifting the spectrum of gold nanoparticle to red or blue region according to the practical environment and satisfy users' special requirement.

3.5. Specificity analysis

To examine the specificity of this proposed HS-Apt@AuNPs colorimetric sensor for assay of *E. coli* O157:H7, the interferences of common bacteria were investigated on a series of other bacteria such as staphylococcus aureus, pseudomonas aeruginosa and *E. coli*ATCC35218 under the same concentration condition (1000 CFU/mL). $MgCl_2$ and HCl were used as triggers since they could produce the spectral shift of HS-Apt@AuNPs colloid to opposite direction for comparison. As shown in Fig. 8, the differential extinction ratio induced by the presence of *E. coli* O157:H7 was much larger than those of other bacteria. Although differential extinction ratio of pseudomonas aeruginosa detected by$MgCl_2$ used as trigger is a little higher than that of its counterpart, its magnitude is still below 20 % compared to that of *E. coli* O157:H7. This result indicates the proposed HS-Apt@AuNPs colorimetric sensor could determine target bacteria with high specificity.

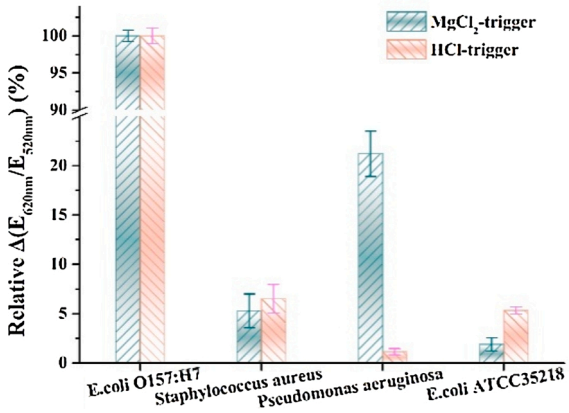

Fig. 8. Specificity of HS-Apt@AuNPs based colorimetric assay with different bacteria of 1000 CFU/mL.

3.6. Binding analysis of aptamers

Mismatched nucleotides functionalized gold nanoparticles were used to compare the specificity of aptamer to *E. coli* O157:H7 under the same procedures as described above. There are two stem-loop structures and some flanking sequences existing in the original 72-mer aptamer. Some studies have shown that the region of stem-loop structure, G-quartet loops, bulges and /or pseudo knots with specific secondary structures have a great contribution to the direct binding with the target molecules [30]. Therefore, mismatched base pairs were designed at these two stem-loop structures to provide three different kinds of control nucleotides, including 5-based mismatched strand (H1), 10-based mismatched strand (H2) and 20-based mismatched strand (H3). Their predicated secondary structures obtained from Mfold web server were shown in Fig. S3. As shown in Fig. 9, the differential extinction ratio $\Delta(E_{620nm}/E_{520nm})$ produced by the original 72-mer aptamer functionalized gold nanoparticles is much higher than its three counterparts, which revealed the specificity to *E. coli* O157:H7 of 72–mer nucleotides with mismatched base pairs was significantly reduced.

3.7. Detection of E. coli O157:H7 in the spiked water samples

To further evaluate the applicability of this proposed biosensor for detection of *E. coli* O157:H7 in water samples, tap water spiked with different concentrations of *E. coli* O157:H7 were prepared. The detection of *E. coli* O157:H7 using this proposed HS-Apt@AuNPs colorimetric sensor was carried out by using $MgCl_2$ and HCl as triggers under the optimal conditions respectively. As show in Table 1, the recoveries for

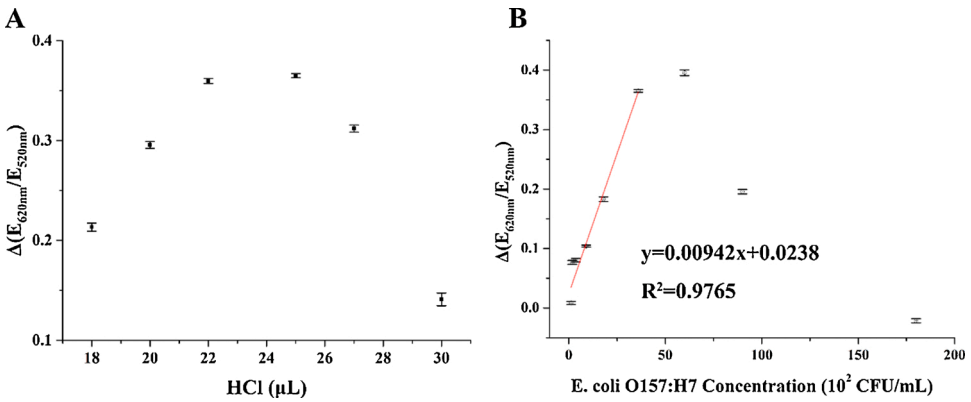

Fig. 7. (A) The effect of volumes of HCl (1.0 M) used as trigger on detecting *E. coli* O157:H7of 3.6×10^3 CFU/mL. (B) Differential extinction ratio, $\Delta(E_{620nm}/E_{520nm})$, as a function of *E. coli* O157:H7concentrations when 25 μL HCl was selected as trigger. The straight line is a linear regression between 1.2×10^2 CFU/mL and 3.6×10^3 CFU/mL of *E. coli* O157:H7.

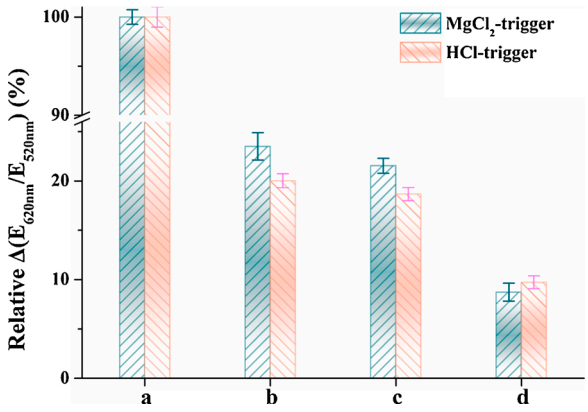

Fig. 9. Differential extinction ratio, Δ(E620 nm/E520 nm), respond to 1000 CFU/mL *E. coli* O157:H7 of gold nanoparticle functionalized by original 72-mer aptamer (a), 5-based mismatched strand (b), 10-based mismatched strand (c) and 20-based mismatched strand (d).

different concentrations (2.0×10^2–3.2×10^3CFU/mL) of *E. coli* O157:H7 in tap water sample ranged from 90.2 %–115 %, and the RSD was in the range of 4.02 %–8.45 %. This indicates that this proposed biosensor was applicable for detection of *E. coli* O157:H7 in water sample.

In addition, the detection result of mixed bacteria in spiked water is shown in Table 2. The average recoveries for 5.0×10^2 CFU/mL and 1.0×10^3 CFU/mL of *E. coli* O157:H7 in tap water sample were 5.1×10^2 CFU/mL and 1.075×10^3 CFU/mL respectively. The RSD was in the range of 6.43 %–9.52 %. The detected concentration of *E. coli* O157:H7 in mixture is acceptable, which indicates this method is able to distinguish *E. coli* O157:H7 from other bacteria.

3.8. Influence on the assays

It is interesting to noted that in the case of HCl used as trigger for HS-Apt@AuNPs colorimetric sensor, the differential extinction ratio $\Delta(E_{620nm}/E_{520nm})$ as a function of *E. coli* O157:H7 concentrations shown in Fig. 7B exhibited a critical point at *E. coli* O157:H7 of 6.0×10^3 CFU/mL. Further addition of *E. coli* O157:H7 provoked the movement of HS-Apt@AuNPs colloid to change from aggregation to dispersion and consequently an decrease in the magnitude of $\Delta(E_{620nm}/E_{520nm})$. This response is different from these cases as shown in Figs. 5B and 6 B. When HS-Apt@AuNPs colorimetric sensor used for *E. coli* O157:H7 is initiated by using $MgCl_2$ and NaOH as trigger, HS-Apt@AuNPs colloid disperse and the differential extinction ratio $\Delta(E_{620nm}/E_{520nm})$ monotonically change with an increase in *E. coli* O157:H7 concentration.

Kim et al. [29] reported that the isoelectric point of *E. coli* O157:H7 is approximately in the range of 3.0–4.2.Under the condition of HCl used as trigger, this pH value of solvent was slightly lower than the isoelectric point of *E. coli*O157:H7 [20,31]. Negative charged HS-Apt@AuNPs could be attracted to tightly immobilized on the positive charged *E. coli* O157:H7 bacterial surface. In contrast, under the condition of $MgCl_2$ and NaOH used as trigger, significant blue-shifted spectra of negative charged HS-Apt@AuNPs stimulated by negative charged *E. coli* O157:H7 had been observed as well, which is different from Su's report that no obvious color changes was observed from the mixing of citrate-capped gold nanoparticles and *E. coli* O157:H7 [32].Thus, a hypothesis is proposed to explain this detection strategy as shown in Scheme 1. The aggregation/dispersion of HS-Apt@AuNPs is comprehensively caused by the pH-dependent electrostatic interaction and the contribution of aptamer. pH is an important factor to determine the spectral shift of HS-Apt@AuNPs colloids. The resonance wavelength of HS-Apt@AuNPs suspension with the presence of *E. coli* O157:H7 could be tuned in the range from 520 to 580 nm by adjusting the volume of pH dependent trigger. Then, why does the critical point only exhibit in the case of HCl used as trigger for HS-Apt@AuNPs colorimetric sensor? In order to investigate the reason for the appearance of this critical point in the case of HCl-trigger typed HS-Apt@AuNPs colorimetric sensor, 30, 45, 70 μL HS-Apt@AuNPs and 18, 25, 30 μLHCl were utilized to evaluate the response of HS-Apt@AuNPs colorimetric sensor to different concentrations of *E. coli* O157:H7ranging from 1.8×10^3 to 1.8×10^4 CFU/mL respectively. As shown in Fig. 10A, it is found that 70 μL HS-Apt@AuNPs lead to a stronger optical response and shift of critical point from lower *E. coli* O157:H7 concentration to higher concentration region compared to the effect of smaller volume of HS-Apt@AuNPs. Moreover, higher volume of HCl resulted in the exhibition of critical point at lower *E. coli* O157:H7 concentration region as shown in Fig. 10B. The pH of mixture shown in Fig. 10A was in the range of 1.67–2.23 due to the addition of HCl. To further investigate the performance of differential extinction ratio $\Delta(E_{620nm}/E_{520nm})$ in the pH range of 3.0–7.0, and avoid the limitation due to the selection of HCl and $MgCl_2$, 0.05 M acetate buffer was utilized to adjust pH and 0.1 M NaCl was used as trigger to initiate detection. By comparing the differential extinction ratio $\Delta(E_{620nm}/E_{520nm})$ resulted from the deionized water with addition of *E. coli* O157:H7 ranging from $1.5 \times 10^3$to 6.0×10^3 CFU/mL as show in Fig. 10C, only the mixture with pH 3 could provide aggregation of HS-Apt@AuNPs colloids. These results reveal that pH imparts the color changing direction of a-ssDNA&AuNPs typed sensor.

Under the condition of pH less than 3, *E. coli* O157:H7 bacteria exhibit positive charged. The volume of HS-Apt@AuNPs determines its quantity in solvent. At a certain volume of HS-Apt@AuNPs, the presence of *E. coli* O157:H7 bacteria initiate the attachment of HS-Apt@AuNPs to

Table 1
Detection of *E. coli* O157:H7 in spiked tap water using the proposed biosensor.

Samples	Spiked concentration	$MgCl_2$-trigger detection			HCl-trigger detection		
		Detected concentration (CFU/mL)	Recovery (%)	RSD (%)	Detected concentration (CFU/mL)	Recovery (%)	RSD (%)
Spiked tap water samples	2.0×10^2	1.8×10^2	90.2	8.45	2.3×10^2	115	8.12
	8.0×10^2	7.5×10^2	93.8	7.74	8.1×10^2	101	5.74
	3.0×10^3	2.9×10^3	96.7	4.02	3.2×10^3	107	3.30

Table 2
Detection of *E. coli* O157:H7 in mixed bacteria tap water using this proposed biosensor.

Samples	Spiked concentration	$MgCl_2$-trigger detection			HCl-trigger detection		
		Detected concentration (CFU/mL)	Recovery (%)	RSD (%)	Detected concentration (CFU/mL)	Recovery (%)	RSD (%)
Spiked tap water samples	5.0×10^2	4.7×10^2	94.0	6.43	5.5×10^2	110	9.52
	1.0×10^3	9.5×10^2	95.0	8.15	1.2×10^3	120	6.92

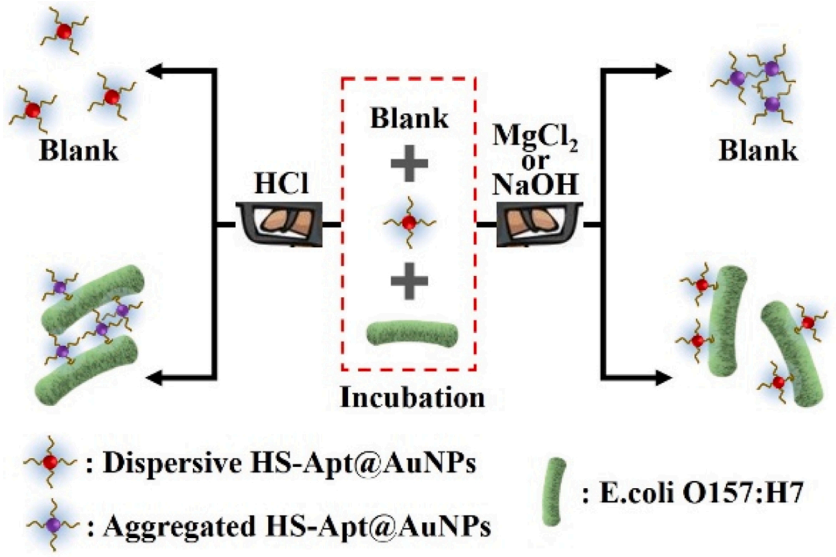

Scheme 1. Schematic representation of HS-Apt@AuNPs based colorimetric sensor for the detection of *E. coli* O157:H7 with various triggers.

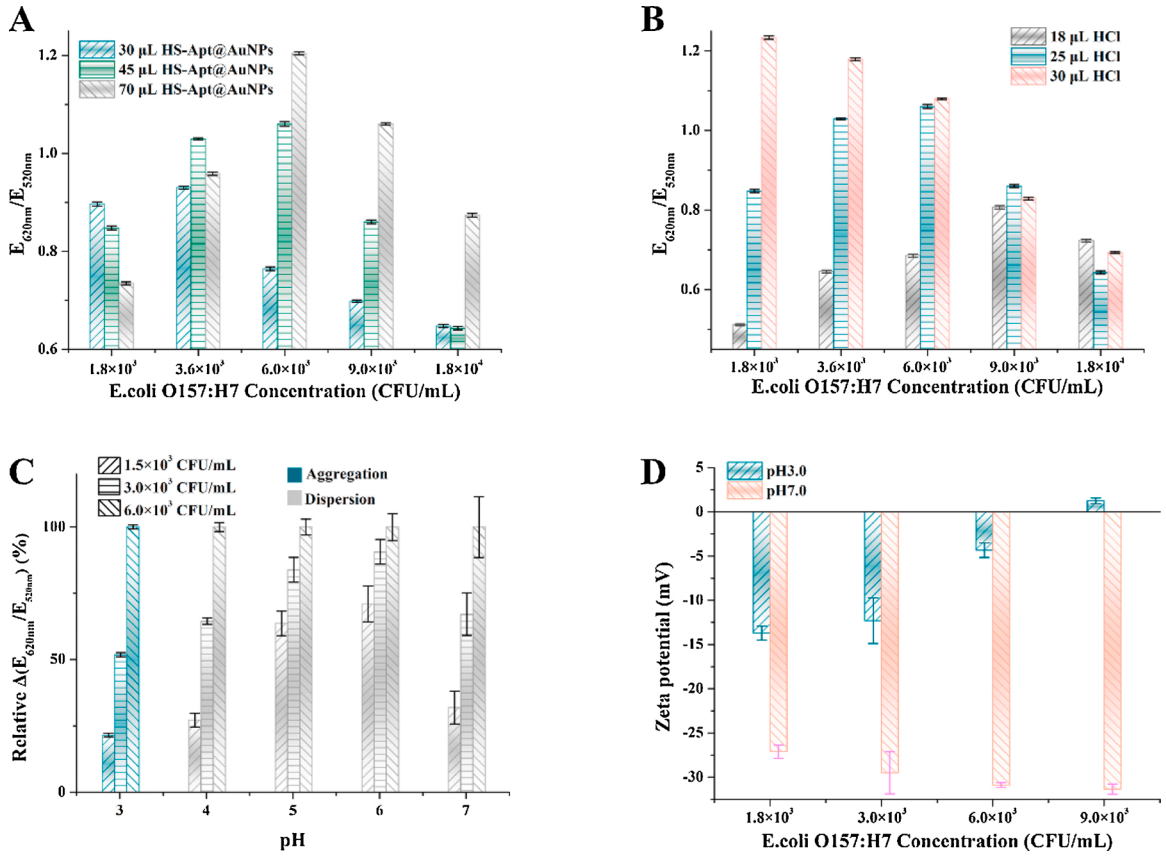

Fig. 10. The volume effects of HS-Apt@AuNPs (A) and HCl (B) on the performance of HS-Apt@AuNPs based colorimetric sensor for the detection of *E. coli* O157:H7with HCl used as trigger. (C)Relative $\Delta(E_{620nm}/E_{520nm})$as a function of pH adjusted by 0.05 M acetate buffer and 0.1 M NaCl. (D) The zeta potential of HS-Apt@AuNPs mixed with different concentrations of *E. coli* O157:H7under pH 3.0 and pH 7.0.

E. coli O157:H7 cells. Due to the fact that the size of *E. coli* O157:H7 bacteria are at least 40 times larger than that of HS-Apt@AuNPs, millions of HS-Apt@AuNPs conjugate with one *E. coli* O157:H7 bacterium, and the aggregation of HS-Apt@AuNPs is thereby produced [32,33]. More and more HS-Apt@AuNPs are mobilized to attach on *E. coli* O157:H7 bacteria until the concentration of *E. coli* O157:H7 approaches one certain level. Once the quantity of *E. coli* O157:H7 bacteria pass this critical concentration, no more HS-Apt@AuNPs are available to conjugate with *E. coli* O157:H7.The function of additional injection of *E. coli* O157:H7 bacteria is to dilute the mixture and electrostatically repulse each HS-Apt@AuNPs/*E. coli* O157:H7 complex, which results in blue-shift of HS-Apt@AuNPs colloids. Moreover, more addition of HCl volume would further decrease the pH of mixture, then *E. coli* O157:H7 bacteria is made to be more positive charged. The accelerated

conjugation rate of HS-Apt@AuNPs on *E. coli* O157:H7 bacteria lead the critical point to be present at a lower *E. coli* O157:H7 concentration region.

On the contrary, the utilization of $MgCl_2$, NaOH and acetate buffer as trigger results in higher pH and negative charged *E. coli* O157:H7 bacteria. Electrostatic repulsion between HS-Apt@AuNPs and *E. coli* O157:H7 cause more steric hindrance on the surface of *E. coli* O157:H7 bacteria and less HS-Apt@AuNPs to participate in the formation of HS-Apt@AuNPs/*E. coli* O157:H7 complex even if the aptamer is prefer to bridge them. The presence of negative charged HS-Apt@AuNPs/*E. coli* O157:H7 complex accelerates their dispersion and shifts the spectrum of HS-Apt@AuNPs colloids to shorter wavelength region until all available HS-Apt@AuNPs are mobilized. As a consequence, differential extinction ratio $\Delta(E_{620nm}/E_{520nm})$ is increased corresponding to the concentration of *E. coli* O157:H7, and then reaches an saturation when the concentration of *E. coli* O157:H7 is more than 6.0×10^3 CFU/mL.

To further explore the electrostatic interactions between HS-Apt@AuNPs and *E. coli* O157:H7 bacteria perturbed by pH, the zeta potential for HS-Apt@AuNPs/*E. coli* O157:H7 complex in various *E. coli* O157:H7 concentration was measured at pH 3 and 7 respectively, and the results are shown in Fig. 10D. At pH 3, the zeta potential, a measure of surface net charge of HS-Apt@AuNPs/*E. coli* O157:H7 complex, was about −14 mV when the *E. coli* O157:H7 concentration is 1.8×10^3 CFU/mL. Then, increasing *E. coli* O157:H7 bacteria gradually neutralizes the overall surface charge and finally gives the complex a positive zeta potential at *E. coli* O157:H7 concentration of 9×10^3 CFU/mL. When the pH of solvent was adjusted to be 7, the negative zeta potential become lower and lower with *E. coli* O157:H7 concentration increasing from 1.8×10^3 to 9×10^3 CFU/mL. This result coincides with the above-mentioned mechanism that surface charge of HS-Apt@AuNPs and *E. coli* O157:H7 bacteria under different pH environments are adjustable in terms of the quantity of HS-Apt@AuNPs and *E. coli* O157:H7 bacteria.

According to the above optical analysis, the following conclusions can be reached. Aptamer and electrostatic interaction comprehensively contribute to the formation of HS-Apt@AuNPs/*E. coli* O157:H7 complex. Aptamer anchored on gold nanoparticle provides high affinity to *E. coli* O157:H7 bacteria whereas pH-dependent charge of HS-Apt@AuNPs and *E. coli* O157:H7 bacteria determine their electrostatic attractive or repulsive interaction. The movement direction of HS-Apt@AuNPs is determined by the quantity of both charged HS-Apt@AuNPs and *E. coli* O157:H7 bacteria. The charge-reversible property of HS-Apt@AuNPs/*E. coli* O157:H7 complex could be designed and utilized for the detection of *E. coli* O157:H7 bacteria under a flexible condition.

4. Conclusion

In summary, a colorimetric biosensor based on aptamer functionalized gold nanoparticles has been developed for the sensitive and selective detection of *E. coli* O157:H7. pH-dependent interaction of gold nanoparticle and *E. coli* O157:H7 has been investigated by using different triggers with pH ranging from acid to alkaline. The triggers with a wide pH range provide an opportunity to modulate the surface net charge of complex consist of aptamer-functionalized gold nanoparticle and *E. coli* O157:H7 bacteria. The quantitative competition between both charged gold nanoparticle and charged *E. coli* O157:H7 bacteria lead the aggregation or dispersion processes of gold nanoparticle. This present study provides a new avenue for a rapid, convenient and cost-effective detection of *E. coli* O157:H7 in practical application. The advantage of this assay is that both the properties of aggregation and dispersion process of gold nanoparticle have been explored for quantitative detection of *E. coli* O157:H7. It enables researcher to design colorimetric biosensor for detection of variety of foodborne pathogen or biomarkers at a more flexible way for specific diagnostics.

CRediT authorship contribution statement

Yuanyang Xie: Methodology, Formal analysis, Investigation, Writing - original draft. **Yu Huang:** Conceptualization, Investigation, Writing - review & editing, Supervision, Funding acquisition. **Jiye Li:** Investigation. **Jiangling Wu:** Resources, Data curation, Project administration.

Declaration of Competing Interest

The authors declare that they have no known competing financial interests or personal relationships that could have appeared to influence the work reported in this paper.

Acknowledgement

This work is sponsored by the Natural Science Foundation of Chongqing (Grant No. cstc2018jcyjAX0718, cstc2018jcyjAX0251).

Appendix A. Supplementary data

Supplementary material related to this article can be found, in the online version, at doi:https://doi.org/10.1016/j.snb.2021.129865.

References

[1] M.A.M. Mahmoud, R.S. Zaki, H.H. Abd-Elhafeez, An epifluorescence-based technique accelerates risk assessment of aggregated bacterial communities in carcass and environment, Environ. Pollut. 260 (2020), 113950.
[2] M. Zhang, T. Bu, Y. Tian, X. Sun, Q. Wang, Y. Liu, et al., Fe3O4@CuS-based immunochromatographic test strips and their application to label-free and dual-readout detection of Escherichia coli O157:H7 in food, Food Chem. 332 (2020), 127398.
[3] S. Zhou, C. Lu, Y. Li, L. Xue, C. Zhao, G. Tian, et al., Gold nanobones enhanced ultrasensitive surface-enhanced Raman scattering aptasensor for detecting Escherichia coli O157:H7, ACS Sens. 5 (2020) 588–596.
[4] Y. Li, H. Liu, H. Huang, J. Deng, L. Fang, J. Luo, et al., A sensitive electrochemical strategy via multiple amplification reactions for the detection of E. coli O157: H7, Biosens. Bioelectron. 147 (2020), 111752.
[5] V. Shirshahi, S.N. Tabatabaei, S. Hatamie, R. Saber, Photothermal enhancement in sensitivity of lateral flow assays for detection of E-coli O157:H7, Colloids Surf. B Biointerfaces 186 (2020), 110721.
[6] M. Esmaelpourfarkhani, K. Abnous, S.M. Taghdisi, M. Chamsaz, A novel turn-off fluorescent aptasensor for ampicillin detection based on perylenetetracarboxylic acid diimide and gold nanoparticles, Biosens. Bioelectron. 164 (2020), 112329.
[7] A.K. Yagati, A. Behrent, S. Beck, S. Rink, A.M. Goepferich, J. Min, et al., Laser-induced graphene interdigitated electrodes for label-free or nanolabel-enhanced highly sensitive capacitive aptamer-based biosensors, Biosens. Bioelectron. 164 (2020), 112272.
[8] J. Sun, Y. Lu, L. He, J. Pang, F. Yang, Y. Liu, Colorimetric sensor array based on gold nanoparticles: design principles and recent advances, TrAC Trends Anal. Chem. 122 (2020), 115754.
[9] Q. You, X. Zhang, F.-G. Wu, Y. Chen, Colorimetric and test stripe-based assay of bacteria by using vancomycin-modified gold nanoparticles, Sens. Actuators B: Chem. 281 (2019) 408–414.
[10] T.H. Kang, C.M. Jin, S. Lee, I. Choi, Dual mode rapid plasmonic detections of chemical disinfectants (CMIT/MIT) using target-mediated selective aggregation of gold nanoparticles, Anal. Chem. 92 (2020) 4201–4208.
[11] Y. Qi, Y. Chen, F.-R. Xiu, J. Hou, An aptamer-based colorimetric sensing of acetamiprid in environmental samples: convenience, sensitivity and practicability, Sens. Actuators B: Chem. 304 (2020), 127359.
[12] X. Ma, Z. Guo, Z. Mao, Y. Tang, P. Miao, Colorimetric theophylline aggregation assay using an RNA aptamer and non-crosslinking gold nanoparticles, Mikrochim. Acta 185 (2017) 33.
[13] G. Yao, J. Li, Q. Li, X. Chen, X. Liu, F. Wang, et al., Programming nanoparticle valence bonds with single-stranded DNA encoders, Nat. Mater. (2019).
[14] Y. Wang, S.L. Kong, X.D. Su, A centrifugation-assisted visual detection of SNP in circulating tumor DNA using gold nanoparticles coupled with isothermal amplification, RSC Adv. 10 (2020) 1476–1483.
[15] Y. Xie, Y. Huang, D. Tang, H. Cui, L. Yang, H. Cao, et al., Sensitive colorimetric detection for lysozyme based on the capture of a fixed thiol-aptamer on gold nanoparticles, New J. Chem. 43 (2019) 4531–4538.
[16] K. Sun, N. Xia, L. Zhao, K. Liu, W. Hou, L. Liu, Aptasensors for the selective detection of alpha-synuclein oligomer by colorimetry, surface plasmon resonance and electrochemical impedance spectroscopy, Sens. Actuators B: Chem. 245 (2017) 87–94.

[17] M. Larguinho, R. Canto, M. Cordeiro, P. Pedrosa, A. Fortuna, R. Vinhas, et al., Gold nanoprobe-based non-crosslinking hybridization for molecular diagnostics, Expert Rev. Mol. Diagn. 15 (2015) 1355–1368.
[18] H. Li, L. Rothberg, Colorimetric detection of DNA sequences based on electrostatic interactions with unmodified gold nanoparticles, Proc. Natl. Acad. Sci. 101 (2004) 14036–14039.
[19] Y. Gan, T. Liang, Q. Hu, L. Zhong, X. Wang, H. Wan, et al., In-situ detection of cadmium with aptamer functionalized gold nanoparticles based on smartphone-based colorimetric system, Talanta 208 (2020), 120231.
[20] Y. Xie, Y. Huang, D. Tang, H. Cui, H. Cao, A competitive colorimetric chloramphenicol assay based on the non-cross-linking deaggregation of gold nanoparticles coated with a polyadenine-modified aptamer, Mikrochim. Acta 185 (2018) 534.
[21] W. Zhao, W. Chiuman, J.C. Lam, S.A. McManus, W. Chen, Y. Cui, et al., DNA aptamer folding on gold nanoparticles: from colloid chemistry to biosensors, J. Am. Chem. Soc. 130 (2008) 3610–3618.
[22] J.G. Bruno, M.P. Carrillo, T. Phillips, C.J. Andrews, A novel screening method for competitive FRET-aptamers applied to E. coli assay development, J. Fluoresc. 20 (2010) 1211–1223.
[23] J. Liu, Y. Lu, Preparation of aptamer-linked gold nanoparticle purple aggregates for colorimetric sensing of analytes, Nat. Protoc. 1 (2006) 246–252.
[24] X. Liu, M. Atwater, J. Wang, Q. Huo, Extinction coefficient of gold nanoparticles with different sizes and different capping ligands, Colloids Surf. B Biointerfaces 58 (2007) 3–7.
[25] J.H. Park, J.Y. Byun, H. Jang, D. Hong, M.G. Kim, A highly sensitive and widely adaptable plasmonic aptasensor using berberine for small-molecule detection, Biosens. Bioelectron. 97 (2017) 292–298.
[26] B.L. Li, L.Y. Peng, H.L. Zou, L.J. Li, H.Q. Luo, N.B. Li, Layered aggregation with steric effect: morphology-homogeneous semiconductor MoS2 as an alternative 2D probe for visual immunoassay, Small 14 (2018).
[27] S.C. Gopinath, T. Lakshmipriya, K. Awazu, Colorimetric detection of controlled assembly and disassembly of aptamers on unmodified gold nanoparticles, Biosens. Bioelectron. 51 (2014) 115–123.
[28] J.A. Jamison, E.L. Bryant, S.B. Kadali, M.S. Wong, V.L. Colvin, K.S. Matthews, et al., Altering protein surface charge with chemical modification modulates protein–gold nanoparticle aggregation, J. Nanopart. Res. 13 (2010) 625–636.
[29] H.N. Kim, Y. Hong, I. Lee, S.A. Bradford, S.L. Walker, Surface characteristics and adhesion behavior of Escherichia coli O157:H7: role of extracellular macromolecules, Biomacromolecules 10 (2009) 2556–2564.
[30] M. Jia, J. Sha, Z. Li, W. Wang, H. Zhang, High affinity truncated aptamers for ultra-sensitive colorimetric detection of bisphenol A with label-free aptasensor, Food Chem. 317 (2020), 126459.
[31] H. Zhang, F.F. Liu, S.C. Wang, T.Y. Huang, M.R. Li, Z.L. Zhu, et al., Sorption of fluoroquinolones to nanoplastics as affected by surface functionalization and solution chemistry, Environ. Pollut. 262 (2020), 114347.
[32] H. Su, Q. Ma, K. Shang, T. Liu, H. Yin, S. Ai, Gold nanoparticles as colorimetric sensor: a case study on E. coli O157:H7 as A model for Gram-negative bacteria, Sens. Actuators B: Chem. 161 (2012) 298–303.
[33] S. Wang, A.K. Singh, D. Senapati, A. Neely, H. Yu, P.C. Ray, Rapid colorimetric identification and targeted photothermal lysis of Salmonella bacteria by using bioconjugated oval-shaped gold nanoparticles, Chem.-Eur. J. 16 (2010) 5600–5606.

Yuanyang Xie received his B.Eng. degree in Environmental Science from Northwest University, China in 2016, M.Sc degree in Environmental Engineering from University of Chinese Academy of Science at 2019. At present, Mr Xie is a PhD candidate at the King's College London, UK. Mr Xie's research interest is focus on the synthesis and application of nanostructure.

Yu Huang received the B.Eng. degree in Automation from Beijing Technology and Business University, China in 2004, M.Sc. in Electronic Communications and Computer Engineering with distinction and Ph.D. in Electrical and Electronic Engineering from the University of Nottingham, UK in 2005 and 2010 respectively. In 2010–2011, he worked in the Institute of Optics and Electronics, Chinese Academy of Sciences. From June 2011, Dr. Huang works in Chongqing Institute of Green and Intelligent Technology, Chinese Academy of Sciences. His research interest is to develop plasmon resonance sensing technology and clinical POCT device.

Jiye Li received the B.Eng degree in Environmental Engineering from Liaoning Shihua University, China in 2018. Currently, Mr Li is pursing his Master degree in Environmental Science at the University of Chinese Academy of Science.

Jiangling Wu received his B.Eng and M.Sc degree in Clinical and Laboratory Diagnosis from Chongqing Medical University in 2014 and 2017 respectively. At present, Mr Wu is pursing his Doctor degree at Chongqing Medical University. Meanwhile, Mr Wu is currently a clinical pathologist at University-Town Hospital of Chongqing Medical University and his research interest is to develop simple and easy-to-use POCT.